Distinguishing Raman from strongly coupled Brillouin amplification for short pulses

Qing Jia,[1] Ido Barth,[2] Matthew R. Edwards,[3] Julia M. Mikhailova,[3,4] and Nathaniel J. Fisch[1,2]
[1]*Department of Astrophysical Sciences, Princeton University, Princeton, New Jersey 08540, USA*
[2]*Princeton Plasma Physics Laboratory, Princeton, New Jersey 08543, USA*
[3]*Department of Mechanical and Aerospace Engineering, Princeton University, Princeton, New Jersey 08540, USA*
[4]*Prokhorov General Physics Institute, Russian Academy of Sciences, 119991 Moscow, Russia*

(Received 27 February 2016; accepted 9 May 2016; published online 26 May 2016)

Plasma-based amplification by strongly coupled Brillouin scattering has recently been suggested for the compression of a short seed laser to ultrahigh intensities in sub-quarter-critical-density plasmas. However, by employing detailed spectral analysis of particle-in-cell simulations in the same parameter regime, we demonstrate that, in fact, Raman backscattering amplification is responsible for the growth and compression of the high-intensity, leading spike, where most of the energy compression occurs, while the ion mode only affects the low-intensity tail of the amplified pulse. The critical role of the initial seed shape is identified. A number of subtleties in the numerical simulations are also pointed out. *Published by AIP Publishing.* [http://dx.doi.org/10.1063/1.4951027]

I. INTRODUCTION

The development of the next generation of ultra-high power (exawatt and greater) lasers is limited by the compression-grating intensity threshold of current chirped pulse amplification systems.[1–3] One proposed method for avoiding this intensity constraint is to use plasma as the amplification medium for late-stage amplifiers. The leading mechanism for plasma-based amplification is resonant stimulated Raman backscattering (SRS),[4–8] where a long pump pulse delivers energy to a counterpropagating short seed pulse through the electron plasma wave. The amplified pulse may be compressed to a duration of order ω_{pe}^{-1}, where $\omega_{pe} = (4\pi n_e e^2/m_e)^{1/2}$ is the electron plasma frequency; n_e, m_e, and e are the electron density, mass, and electric charge, respectively. Optimal parameter regimes for robust and efficient SRS amplification have been explored in depth,[9,10] and verified numerically and experimentally.[11–21]

Amplification via stimulated Brillouin scattering (SBS), where the ion-acoustic wave mediates energy transfer, has been proposed as an alternative to SRS,[22] with particular attention given to the strongly coupled SBS (SC-SBS) regime.[23,24] In the SC-SBS regime, the ion-wave is a driven quasi-mode whose frequency depends on the laser strength, and the minimum compressed pulse duration is claimed to be only of the order of the inverse ion plasma frequency, $\omega_{pi}^{-1} = (4\pi n_i Z^2 e^2/m_i)^{-1/2}$ (here, n_i, m_i, and Ze are the ion density, mass, and electric charge, respectively), rather than the ion acoustic period as in the weak-coupling SBS regime.[22] Possibly, the limitation is given by the characteristic frequency of the SC-SBS mode,[25] but in either case, these are long durations compared to the minimum duration expected in SRS. On the other hand, unlike SRS, which is limited to densities below one-quarter of the critical density, $n_{cr} = m_e\omega_0^2/4\pi e^2$ (ω_0 is the laser frequency), SBS is possible in all sub-critical-density plasmas.

It has been reported that SC-SBS amplification and compression in $0.3\,n_{cr}$ density plasmas have been demonstrated via one dimensional (1D) particle-in-cell (PIC) simulations.[22] In addition, SC-SBS amplifiers were also studied analytically and numerically using fluid model and Vlasov simulations.[26–30] Due to laser filamentation at higher densities, it has been suggested that SC-SBS should be employed for amplification at smaller, sub-quarter-critical plasma densities, $N = n_e/n_{cr} \leq 0.25$, where SRS may also occur.[25,31–34]

It is thought that the main advantage of SC-SBS over SRS amplifiers is that the pump and seed may have the same frequency.[25,32] This is because the frequency shift (ω_{plasma}) associated with the three-wave resonance condition, $\omega_{pump} = \omega_{seed} + \omega_{plasma}$, is negligible compared to the laser frequency for SC-SBS but not for SRS. Relying on the premise that the type of amplification is dictated by the initial frequency of the seed, amplification for equal pump and initial seed frequencies in sub-quarter-critical-density plasma was previously attributed primarily to SC-SBS, with only cursory mention that due to the frequency spread of ultra-short pulses, both SRS and SC-SBS might contribute simultaneously to the amplification.[25,32]

Here, we aim to distinguish the separate contributions of SRS and SC-SBS for amplification of short pulses in the regime $0.01 \leq N \leq 0.05$, using 1D PIC simulations to study the amplification dynamics when seed and pump have the same frequency. Here, by SRS, we mean electron-based scattering only, which encompasses the resonant Raman scattering effect, whether in the wavebreaking regime or not, and the resonant Compton-like superradiant amplification effect, where the electron motion is determined by the ponderomotive force rather than by the collective plasma wave electric field.[4,35,36] The main point is that SRS is mediated by electrons only, with ion motion immaterial. For clear comparison, we first revisit the simulations of Ref. 25 for both

mobile and immobile ions. By detailed spectral analysis, we demonstrate that the amplification of the 13 fs seed is entirely due to SRS with little contribution of SC-SBS. For the longer (80 fs) seed, we find that SRS is responsible for the first leading spike amplification, while SC-SBS determines the trailing part of the amplified pulse. From this analysis and previous SRS studies,[37–40] we show that the maximum amplified amplitude is determined by the seed front rather than by its duration (as claimed in Ref. 25). In contrast, the seed duration determines the amplitude of the trailing pulse, which is dominated by SC-SBS.

The paper is organized as follows. Sec. II revisits and reanalyzes the results of Refs. 25 and 32. Sec. III studies the influence of the seed front and duration on the final amplified pulse. Sec. IV discusses noise and resolution effects in the moving-window PIC simulations. Sec. V summarizes the conclusions and provides suggestions for future study in the field.

II. DOMINANT ROLE OF SRS

As has previously been pointed out,[25] the straightforward method to distinguish between SRS and SC-SBS amplification is to compare simulations with mobile and immobile ions, since only the electron mode (SRS) can contribute in the immobile ion simulations, but both the electron and ion modes may contribute in the mobile ion simulations. Previous simulations[25] suggested that for an initial 80 fs pulse, amplification of the leading spike was almost identical in the mobile and immobile ion cases, but a long, low-amplitude trailing pulse grew only in the mobile ion case. The corresponding Fourier spectrum implied that both signals, at ω_0 (which corresponds to SC-SBS) and at $\sim 0.7\omega_0$ (which corresponds to SRS for $N = 0.05$ density plasma), contributed to the head of the pulse, but only SC-SBS was responsible for the tail. For the amplification of an initially 13 fs seed, the temporal field distribution was almost the same for the mobile and immobile ion cases, and it was conjectured[25] that the excitation of mixed SBS-SRS-modes produced the broad spectrum of the amplified seed.

However, it should be noted that all of the temporal and spatial spectral analyses presented in Ref. 25 were based on the Fourier transform of the total magnetic field (B_z), which contains both pump and seed components. Since the initial pump and seed are at frequencies indistinguishable from that produced by SC-SBS, it is easy to overestimate the contribution of SC-SBS amplification to the final signal.

Here, we run simulations replicating the parameters of Refs. 25 and 32 in one-dimension using the explicit full relativistic PIC code EXEMPLAR[41] and EPOCH.[42] We consider a trapezoidal plasma density profile with a plateau density of $N = 0.01$. This is lower than the $N = 0.05$ plateau density of Refs. 25 and 32, since we found that for the typical full-window simulations, which include the modeling of initial pump propagating process as in realistic experiments, the numerical noise induced SRS in the $N = 0.05$ plasma significantly depletes the pump before arrival of the seed. Thousands of particles per cell need to be applied to diminish this unphysical numerical influence, the computing requirement of which is costly. We choose to use the less dense plasma where the premature pump depletion is not so prominent, and the principle amplification mechanism remains the same with the higher density plasma case. The latter is demonstrated by the comparison between the wavevector spectra in simulations using a moving window and 13 fs seed for these two densities, as shown in Fig. 7 in Sec. IV.

To provide a more detailed analysis of the amplified seed spectrum, we decompose the total electromagnetic field into right-propagating (pump) and left-propagating (seed) waves by approximating $E^{\text{right}}_{\text{left}} = E_y \pm v_p B_z$, where $v_p = \omega_0/k_0 = c/(1-N)^{1/2}$ is the phase velocity of the pulses in plasma.[22] Additionally, rather than taking the temporal/spatial Fourier transform over the whole pulse duration/space interval (as in Figs. 6(b) and 8 of Ref. 25), we split the pulse into two time/space intervals, the leading spike and the trailing part (see the region I and region II in Figs. 1(a) and 2(a)).

Figure 1(a) compares the temporal field distributions of the amplified seed pulse obtained in mobile ions (red) and immobile ions (blue) simulations. The spectra of the two time regions for both mobile and immobile simulations are presented in Fig. 1(b). We note that there is almost no difference between the mobile and immobile spectra for the leading spike (region I), which is primarily composed of two components

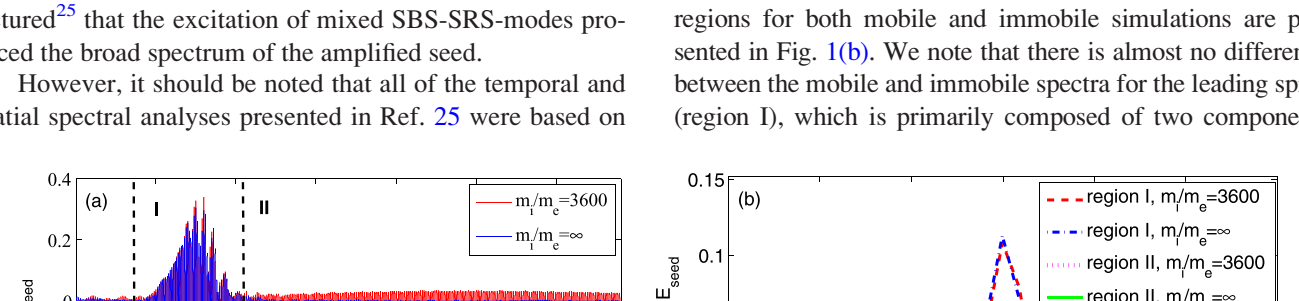

FIG. 1. (a) Temporal electric field structure of the amplified seed pulse for the case with mobile ions (red curve) and immobile ions (blue curve). The electric field amplitude in this paper is normalized to $E_0 \equiv m_e c\omega_0/e$. (b) The corresponding frequency spectra of the waves in different regions shown in (a). The plasma has a trapezoidal density profile with a 240 μm plateau at density $N = 0.01$ and a 240 μm ramp on each side. The plasma is composed of electrons and ions with charge $Z = 1$, mass $m_i = 3600\, m_e$ for mobile ion case. Electron and ion temperatures are 500 eV and 50 eV, respectively. The temporally flat pump intensity is 10^{16} W/cm^2 with a duration of 4.75 ps. The initial maximum intensity of the temporal Gaussian-shape seed is 10^{17} W/cm^2 with a full-width half-maximum (FWHM) duration of 80 fs. The wavelength of both the pump and seed is $\lambda = 1$ μm. Pump and seed first meet at the right plasma boundary. Simulations have a resolution of 100 particles per cell and 50 cells per wavelength. The boundary conditions are open for the lasers and thermal for the particles.

with the central frequencies $\sim\omega_0$ and $\sim 0.82\omega_0$. In contrast, in the trailing part (region II), only the mobile ion case contains a nonzero signal at $\sim\omega_0$ (magenta dotted line), while there is no significant signal for the immobile ion case (green solid line). The fact that the leading spike spectra in the mobile and immobile cases are almost the same, which demonstrates that the pulse amplification is purely due to the electron motion (SRS) while the ion quasi-mode (SC-SBS) alone contributes to the small amplitude tail. The contribution to the spectra near ω_0 in the leading spike is due to the initial seed and must not be misinterpreted as an amplified SC-SBS signal. Only the small contribution, around $0.82\omega_0$, clearly results from plasma SRS amplification. The frequency of this component, if due to resonant Raman scattering, would be $(\omega_0 - \omega_{ek})$ on account of the thermal effect on the plasma wave (here, $\omega_{ek} = \sqrt{\omega_{pe}^2 + 3k^2 v_{te}^2}$, and v_{te} is the electron thermal velocity). This implies an effective electron temperature of about 1.1 keV, which is in reasonable agreement with the electron temperature (about 890 eV) deduced from the simulation result. In addition, note that the laser and plasma parameters in this case also fulfil the superradiant amplification condition, $\omega_B > \omega_{pe}$, where $\omega_B = 2\omega_0\sqrt{a_0 a_1}$ is the electron bouncing frequency in the ponderomotive potential generated by the two counterpropagating pulses.[4,35,36] Here, $a_{0,1} = eA_{0,1}/m_e c^2$ are the normalized vector potentials of the pump and seed pulses, respectively. In this regime, the amplified component frequency is $(\omega_0 - \omega_B)$. The maximum seed amplitude $a_1 = 0.27$ gives the amplified frequency of $0.7\omega_0$, while the amplitude of resonant frequency component $a_{1,\omega=\omega_0} = 0.12$ (see Fig. 3(a)) gives the amplified frequency of $0.8\omega_0$, which is closer to the amplified frequency found in the simulation. In order to distinguish between these two electron-based mechanisms, we artificially turn off the effect of the longitudinal electrostatic field (E_x) on the particle motions in the PIC code. In this case, no Langmuir wave is generated, and the superradiant amplification should be the only contributor to the amplification. However, unlike other typical Raman or superradiant regimes (not shown), for the particular parameters in this case, turning off the E_x effect did not result in a conclusive answer. This might imply contributions of both resonant Raman and Compton-like superradiant amplifications. In either event, what is clear is that the observed amplification of the leading spike is an electron effect only, and not affected by ion dynamics.

Figure 2(a) shows a snapshot of the spatial distributions of the pump, seed, and the electrostatic (E_x) fields for the mobile ion simulation. The small depletion of the pump (blue) behind the amplified seed pulse (green) results from low amplification efficiency in the regime where pump intensity is far beyond the wavebreaking threshold.[5,43,44] Again, we separate the space into the leading spike (region I) and the trailing pulse (region II) according to the amplified seed structure. The results of the spatial Fourier spectrum in the two regions are shown in Figs. 2(b) and 2(d), respectively. The E_x field spectra in the leading spike region clearly show that in addition to the $k = 2k_0$ mode resulting from the beating of the pump ($k = k_0$) and seed ($k = k_0$), another backward SRS mode ($k = 1.82k_0$) is excited which satisfies the resonant condition $k_{\text{seed}}(0.82k_0) + k_{\text{pump}}(k_0) = k_{\text{plasma}}(1.82k_0)$. In contrast, no SRS mode appears in the tail region as shown in Fig. 2(d). Notably, the trailing part includes also a very large Fourier component at $\sim 0.1\ k_0$, which is shown in Fig. 2(c). The associated wavelength, $\sim 2\pi c/\omega_{pe}$, indicates that this mode is driven by the breaking of the Langmuir wave as expected in the wave-breaking regime.[45]

To further clarify the SRS amplification process for the leading spike, we record the left-propagating field at several positions in the amplifier and calculate the Fourier transform of the leading spike. Figure 3(a) displays the evolution of the frequency spectra of the leading spike for the amplification of the initial 80 fs seed in the mobile ion simulation. Remarkably, the initially tiny $\sim 0.82\omega_0$ component is dramatically amplified, while the initially large $\sim\omega_0$ component remains unchanged. Based on the above analysis, we claim that while it is true that the tail is dominated by SC-SBS, only SRS contributes to the leading spike of the amplified pulse.

Finally, let us revisit the ultrashort 13 fs seed amplification case. In agreement with the results of Ref. 25, our simulation exhibits almost the same amplified seed profile for the mobile and immobile ion cases (not shown). Figure 3(b) shows the corresponding frequency spectrum evolution for the mobile ion simulation. Although it is difficult to resolve the detailed Fourier components because of its ultrashort duration, it is notable that the amplification occurs only for the frequency components $\omega < \omega_0$. This agrees with the above spectral analysis of the initial 80 fs seed case in which only the sub-ω_0 Fourier components are amplified.

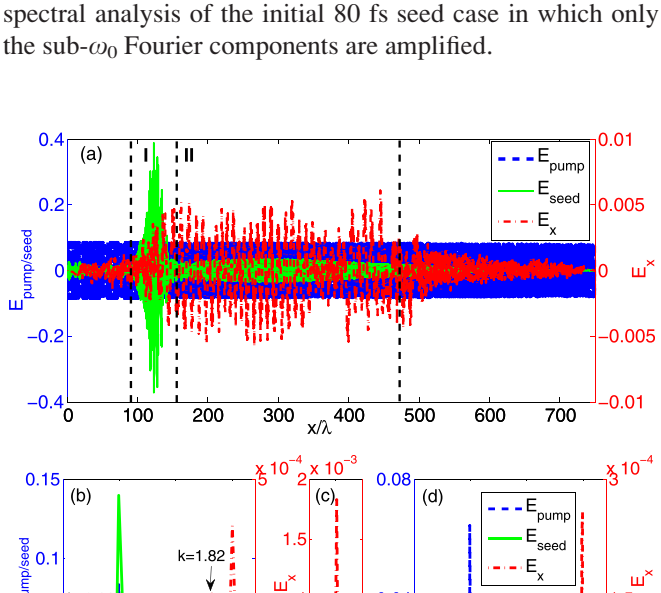

FIG. 2. (a) Spatial distributions of the electric fields of the right-propagating pump (E_{pump}, blue, left axis), left-propagating seed (E_{seed}, green, left axis) and the electrostatic field (E_x, red, right axis) in the plasma (red) at time $t = 4.4$ ps in the mobile ion simulation. (b)–(d) The wave vector spectra of the pump (dashed blue line, left axis), the seed (solid green line, left axis), and the electrostatic wave (dash-dotted line, right axis) of the leading spike region I (b) and of the trailing region II (d). (c) The large-wavelength part of the k spectra of the E_x field in the trailing region II with different scale.

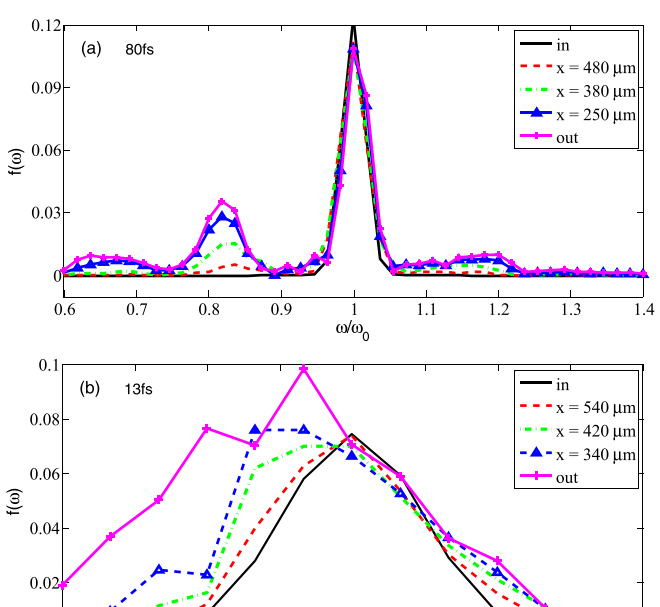

FIG. 3. Frequency spectra evolution of the leading spike of the amplified pulse for the 80 fs seed (a) and the 13 fs seed (b) as collected at different locations in the plasma. The black solid curve is for the input seed, and the magenta curve with plus sign markers is for the output seed.

This completes our demonstration that for the parameter regime addressed in Refs. 25 and 32, SRS alone is the dominant mechanism of the leading spike amplification while SC-SBS is responsible only for the generation of the trailing part of the pulse. Next, we refine the analysis and separate the effects of the seed front shape and seed duration on the amplification process.

III. EFFECTS OF SEED SHAPE

It was found in Refs. 25 and 32 that the highest maximum output intensity is obtained for the shortest seed. Guided by our identification of the intensity maximum being due entirely to SRS, we expect that the rise time of the seed

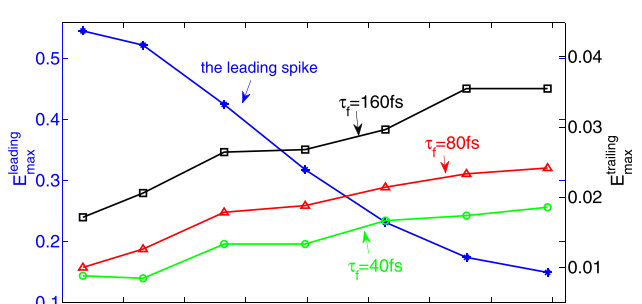

FIG. 5. Maximum amplitudes (left axis) of the final seed leading spike (blue stars) with different rise duration τ_r, and the corresponding maximum amplitudes (right axis) of the trailing part for $\tau_f = 40$ fs (green circles), 80 fs (red triangles), and 160 fs (black squares). Pump and plasma parameters are the same as in Fig. 4.

will be the most important parameter in reaching high-intensity regimes.[37–40] Thus, we carry out several 1D PIC simulations with seeds of different rise time and durations to study the effect of changing seed temporal parameters on the amplification process.

Consider initially trapezoidal seeds with rise-time τ_r and flat-top duration τ_f. Figure 4 shows six different input seed structures (left column), the corresponding leading spike (middle column), and the trailing pulse (right column) structures of the output seed. It is shown that the leading spike and the maximum amplitude of the output seed are the same for the seeds with the same rise time [see (a)–(c) or (d)–(f)], while the increasing of seed duration results in growing of the trailing pulse amplitude. To illustrate these conclusions, we summarize the simulation results in Fig. 5. It is shown that the leading spike maximum (blue stars and left axis) is determined by the seed rise time, in agreement with SRS theory, i.e., sharper seed fronts result in higher maximum amplitudes, which also justify the observed highest amplitude for the shortest seed pulse considering the same Gaussian shape seed.[25,32] It is worth noting that seeds with different durations (τ_f), but the same rise time (τ_r), produce the same leading spike amplification. On the other hand, for the amplification of the trailing part (right axis), the

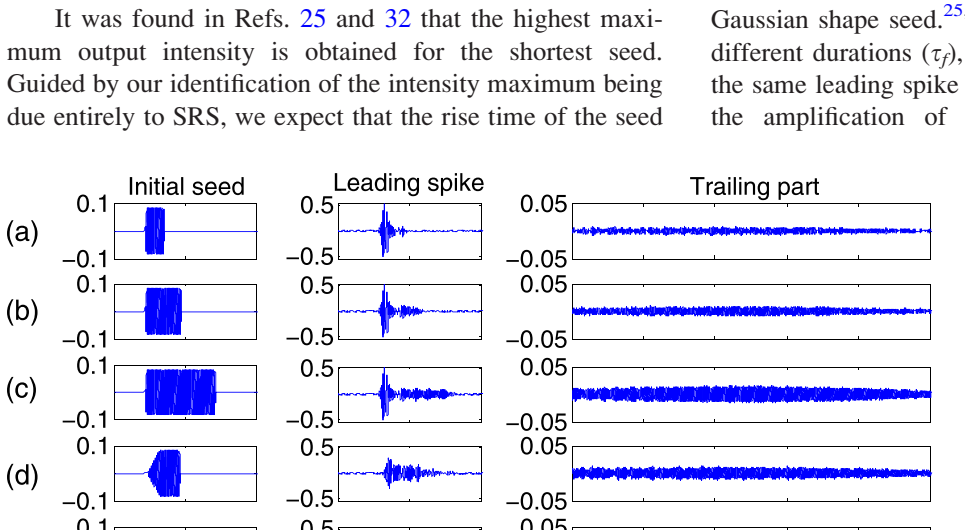

FIG. 4. Simulation results of the output electric field structures of the leading spike (second column) and the trailing pulse (third column) for different initial seed structures (first column). The input seeds in (a)–(c) are of the same sharp rise time $\tau_r = 4$ fs, while (d)–(f) own the same relative mild front $\tau_r = 27$ fs. The plateau durations for (a) and (d), (b) and (e), and (c) and (f) are $\tau_f = 40$, 80, 160 fs, respectively. In all these simulations, the seed and pump are of the same frequency and intensity 10^{16} W/cm^2, and the plasma has a flat density profile of N = 0.01 with a length of 720 μm. All the other simulation parameters are the same as those in the former cases.

comparison of the green circles ($\tau_f = 40$ fs), red triangles ($\tau_f = 80$ fs), and black squares ($\tau_f = 160$ fs) shows increasing amplification with increasing seed duration (the three curves themselves illustrate the same increasing trend for the increasing total duration time), which results in larger total energy transfer efficiency due to enhanced SC-SBS amplification. It is also important to note that for the discussed parameter regime, the total energy deposited in the trailing pulse is much smaller than the energy deposited in the leading spike for all the presented simulations.

IV. EFFECTS OF PARTICLE NOISE AND MOVING WINDOWS

In the regime under consideration ($0.01 \leq \mathrm{N} \leq 0.05$, with pump intensity $I_{\mathrm{pump}} \sim 10^{16}\,\mathrm{W/cm^2}$), the instability growth rates are large and kinetic effects are important; the outcome of amplification is thus remarkably sensitive to choices of physical and non-physical parameters at resolutions far beyond what might ordinarily be considered sufficient. This sensitivity can account both for differences in observed amplification at nominally similar parameters and spurious signals which might be mistaken for Brillouin scattering. It claims that observed differences that are physically significant must therefore be treated with extreme care. In this section, we consider how the choice of ion-immobilization method, whether to use a moving window frame, and the number of particles in a cell affect the outcome of efforts to capture short-pulse amplification with PIC simulations in the regime originally considered in Refs. 25 and 32.

The first choice when using a PIC code to study amplification via stimulated Raman or Brillouin scattering is whether to conduct the simulation in a moving reference frame, i.e., a computational window which encompasses the seed pulse and travels at its speed. A moving window offers the dual benefits of reducing the computational requirements and suppressing the plasma–pump interaction until shortly before the arrival of the seed. The first property is generally useful, but the second can be crucial in regimes where premature pump depletion from PIC noise can render full-domain simulation useless. Since backscattering is induced by particle noise (proportional to $\sqrt{N_{ppc}}$, where N_{ppc} is the number of particles per cell), full-window simulations will tend to overestimate pump pre-depletion. On the other hand, real plasmas contain density fluctuations, so the artificial suppression imposed by a moving window simulation will tend to underestimate premature pump depletion. Physical experiments lie somewhere between these two results. The regime under consideration exhibits sufficiently high growth rates that the choice of whether to use a moving window changes the observed amplification.

Consider, as an example, Fig. 6 shows the maximum intensity of the seed pulse as a function of position in a trapezoidal plasma profile in PIC simulations with and without moving window for mobile and immobile ions. The striking difference in achievable intensity between the moving window and stationary reference frame simulations results primarily from premature backscattering of the pump laser

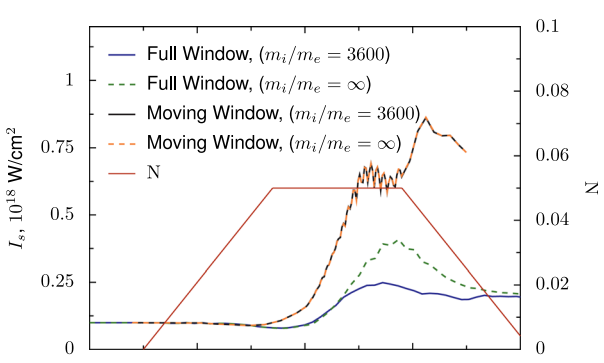

FIG. 6. Maximum intensity of seed pulse with propagation distance for moving window and full-window simulations and mobile (ion mass $m_i = 3600 m_e$) and immobile ions (ions mass to infinity). The electron and ion temperatures are 500 eV and 50 eV, respectively. The Gaussian-shape pump has a maximum intensity of $10^{16}\,\mathrm{W/cm^2}$, a wavelength of 1 μm, and an FWHM duration of 3.2 ps. The initial Gaussian-shape seed maximum intensity is $10^{17}\,\mathrm{W/cm^2}$, wavelength 1 μm, and FWHM duration of 13 fs. Pump and seed first meet at the center of the plasma. The plateau plasma density is $\mathrm{N} = 0.05$. The simulations (EPOCH) have a resolution of 100 cells/λ and 100 particles per cell.

before the arrival of the seed, though plasma disruption also plays a role. In the moving window, the mobile and immobile ion simulations produce identical maximum intensity results, in agreement with the conclusion that the ion dynamics have no effect in the 13 fs timescale of the leading spike. In the longer, trailing component of the pulse, some ion-based amplification can be observed (see the green curves in Fig. 2(a)). The difference between the mobile and immobile ion simulations in the non-moving window can be attributed to premature stimulated Brillouin scattering of the pump, which is substantial because the spontaneous pump–plasma interaction occurs over long spatial and temporal scales.

Figure 7 compares the wavevector spectra of seeds amplified in trapezoidal density profile plasmas with plateau density $\mathrm{N} = 0.01$ and $\mathrm{N} = 0.05$ plasmas in moving window

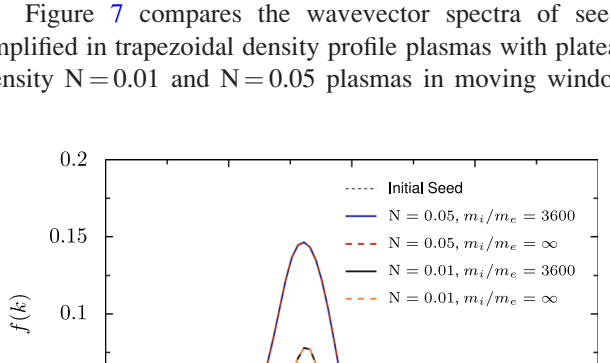

FIG. 7. Comparison of seed wavevector spectra for the leading spike (region I) of the amplified seed in the trapezoidal-density-profile plasma with maximum density $\mathrm{N} = 0.01$ and $\mathrm{N} = 0.05$. The dotted curve shows the original seed wavevector spectra for reference. The overlap of the mobile and immobile ion simulations demonstrates that for both sets of parameters, the ions play no role in the amplification of the peak. Simulation resolution is 100 cells/λ and 800 particles per cell. Other simulation parameters are the same as those in Fig. 6.

simulations. The overlap of both the mobile and immobile ion simulation results demonstrate that ions play no role in the amplification in both density cases. Moreover, the amplification of the sub-ω_0 components is more prominent in the N = 0.05 plasma case, which results from the higher SRS growth rate in the higher plasma density. These qualitatively similar spectra and the pure SRS amplification effects suggest that the detailed analysis performed for N = 0.01 in Sec. II is also applicable to N = 0.05.

The standard method for checking whether observed backscattering is electron or ion driven is to immobilize the ions and run the simulation again under the same parameters; the immediate conclusion is that any difference between the two outcomes will necessarily be the result of the ion mode (see, for example, Fig. 3(b) in Ref. 25). However, care must be taken, because there are multiple methods available for removing ions from the simulations. The obvious method is to set the ion mass to a large number, so that ions are immobile on the timescale of the entire simulation. An appealing alternative is to remove all the ions and replace them with a neutralizing background field, which halves the number of particles, reducing computational costs. However, as Fig. 8(a) shows, a neutralizing background field is not equivalent to immobile ions, and in the studied regime, noticeably different amplification is observed. Compared to the

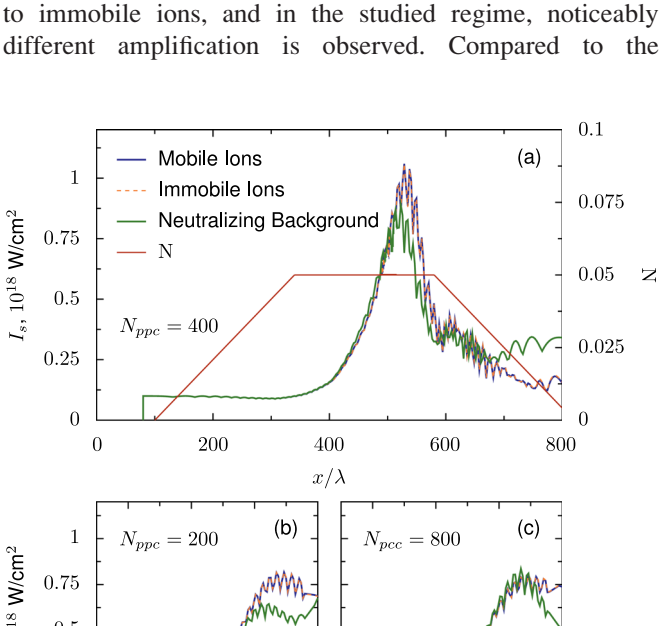

FIG. 8. Comparison of moving-window simulations using two different methods of ion immobilization. (a) The maximum seed intensity produced via amplification with mobile ions ($m_i = 3600m_e$, $T_i = 50$ eV) is compared to a simulation with ions immobilized by setting their mass to infinity and one with ions removed and replaced with a neutral background field. The close agreement between the mobile and immobile cases indicates that the ion dynamics play no role in the amplification. The noticeable difference between the two immobile ion cases demonstrates that static ion effects can be important in this regime, and that the method of ion immobilization matters when trying to identify stimulated Brillouin scattering. (b) and (c) show the maximum seed intensity results of simulations with different numbers of particles per cell. The plateau plasma density is N = 0.05. Simulation resolution is 100 cells/λ. Other simulation parameters are the same as those in Fig. 6.

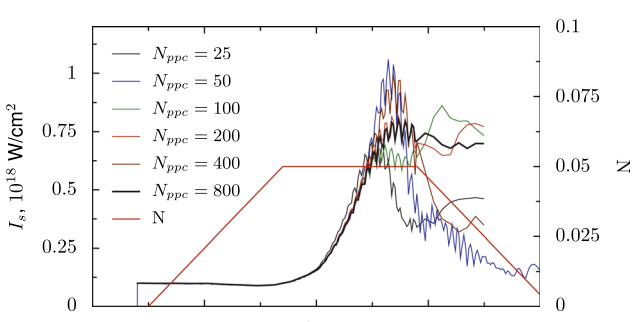

FIG. 9. Comparison of moving-window simulations using different numbers of particles per cell and the neutralizing background field option for immobile ion modeling. This figure demonstrates that in this regime, the simulations are significantly resolution dependent even for very large numbers of particles per cell. The plateau plasma density is N = 0.05. Simulation resolution is 100 cells/λ and 100 particles per cell. Other simulation parameters are the same as those in Fig. 6.

neutralizing background field case, the immobile ion simulation contains random field fluctuations, which can contribute to the apparent amplification. The misleading comparison of the mobile ion and neutralizing background field cases might lead to the conclusion that additional amplification in the mobile ion case is due to the SC-SBS amplification, while in reality, the comparison of the mobile and immobile ion cases gives the same amplification behaviors for the leading spike. As indicated in Figs. 8(b) and 8(c), this effect persists even to relatively high simulation resolutions and cannot generally be assumed negligible.

The above effects should disappear for sufficiently high resolution simulations with large numbers of particles in each cell, because in the fluid (continuum) limit, no distinction can be made between the two immobile ion cases. However, the sensitivity to noise of the instabilities of interest in this regime is such that even at remarkably high numbers of particles per cell ($N_{ppc} > 800$), we still see resolution-dependent behavior (Fig. 9). This is larger than the velocity-space resolution regularly used in this field of research, and it is likely that the resolutions required to truly examine the fluid limit are not practically attainable.

V. SUMMARY

In conclusion, by detailed spatial and temporal spectra analysis of 1D PIC simulations, we demonstrate that contrary to the claims in Refs. 25 and 32, in the regime where $0.01 \leq N \leq 0.05$ and $I_{\text{pump}} = 10^{16}$ W/cm^2, the amplification of the leading spike is driven by electron-based resonant SRS (i.e., Raman or Compton-like superradiant amplification), rather than by ion-based SC-SBS. In this regime, SC-SBS is responsible only for the energy transfer to the low-intensity trailing part. We also find that the seed front sharpness determines the maximal amplification of the leading spike in complete accord with SRS compression theory, while the seed duration contributes only to the trailing part amplification.

Notably, the pump and seed intensities in this regime are so high that both kinetic wavebreaking and relativistic nonlinearity are important.[5,7,46–49] Therefore, complete

understanding of the resonant amplification for plasma densities between $0.01n_{cr}$ and $0.25n_{cr}$ and pump intensities above the wavebreaking threshold requires further kinetic study. Additional open problems in this regime include the effects of pulse and seed initial intensities, ion and electron temperatures, plasma length, and density profile and fluctuations. Further parameter optimization is required for finding the best possible efficiency and the maximum accessible intensity in this regime.

ACKNOWLEDGMENTS

This work was supported by the U.S. DTRA Grant No. HDTRA1-11-1-0037, AFOSR Grant No. FA9550-15-1-0391, NNSA Grant No. DE-NA0002948, and the U.S. DOE Grant No. DE-AC02-09CH1-1466. The authors gratefully acknowledge A. A. Balakin and C. Z. Xiao for the constructive discussions. M.R.E. acknowledges the support of the NSF through a Graduate Research Fellowship. This work was partially performed at PPPL's Research Computing Center and the High Performance Computing Center at Princeton University. The development of the EPOCH code was funded in part by UK EPSRC Grant Nos. EP/G054950/1, EP/G056803/1, EP/G055165/1, and EP/M022463/1.

[1]D. Strickland and G. Mourou, Opt. Commun. **55**, 447 (1985).
[2]G. A. Mourou, C. P. J. Barty, and M. D. Perry, Phys. Today **51**(1), 22 (1998).
[3]I. V. Yakovlev, Quantum Electron. **44**, 393 (2014).
[4]G. Shvets, N. J. Fisch, A. Pukhov, and J. Meyer-ter-Vehn, Phys. Rev. Lett. **81**, 4879 (1998).
[5]V. M. Malkin, G. Shvets, and N. J. Fisch, Phys. Rev. Lett. **82**, 4448 (1999).
[6]V. M. Malkin, G. Shvets, and N. J. Fisch, Phys. Plasmas **7**, 2232 (2000).
[7]V. M. Malkin, Y. A. Tsidulko, and N. J. Fisch, Phys. Rev. Lett. **85**, 4068 (2000).
[8]N. J. Fisch and V. M. Malkin, Phys. Plasmas **10**, 2056 (2003).
[9]D. S. Clark and N. J. Fisch, Phys. Plasmas **10**, 3363 (2003).
[10]V. M. Malkin and N. J. Fisch, Eur. Phys. J. Spec. Top. **223**, 1157 (2014).
[11]Y. Ping, I. Geltner, N. Fisch, G. Shvets, and S. Suckewer, Phys. Rev. E **62**, R4532 (2000).
[12]Y. Ping, I. Geltner, A. Morozov, N. Fisch, and S. Suckewer, Phys. Rev. E **66**, 046401 (2002).
[13]Y. Ping, W. Cheng, S. Suckewer, D. S. Clark, and N. J. Fisch, Phys. Rev. Lett. **92**, 175007 (2004).
[14]A. A. Balakin, D. V. Kartashov, A. M. Kiselev, S. Skobelev, A. N. Stepanov, and G. M. Fraiman, J. Exp. Theor. Phys. Lett. **80**, 12 (2004).
[15]W. Cheng, Y. Avizour, Y. Ping, S. Suckewer, N. J. Fisch, M. S. Hur, and J. S. Wurtele, Phys. Rev. Lett. **94**, 045003 (2005).
[16]R. Kirkwood, E. Dewald, C. Niemann, N. Meezan, S. Wilks, D. Price, O. Landen, J. Wurtele, A. Charman, R. Lindbert *et al.*, Phys. Plasmas **14**, 113109 (2007).
[17]C.-H. Pai, M.-W. Lin, L.-C. Ha, S.-T. Huang, Y.-C. Tsou, H.-H. Chu, J.-Y. Lin, J. Wang, and S.-Y. Chen, Phys. Rev. Lett. **101**, 065005 (2008).
[18]N. Yampolsky, N. Fisch, V. Malkin, E. Valeo, R. Lindberg, J. Wurtele, J. Ren, S. Li, A. Morozov, and S. Suckewer, Phys. Plasmas **15**, 113104 (2008).
[19]Y. Ping, R. Kirkwood, T.-L. Wang, D. Clark, S. Wilks, N. Meezan, R. Berger, J. Wurtele, N. Fisch, V. Malkin *et al.*, Phys. Plasmas **16**, 123113 (2009).
[20]D. Turnbull, S. Li, A. Morozov, and S. Suckewer, Phys. Plasmas **19**, 073103 (2012).
[21]G. Vieux, A. Lyachev, X. Yang, B. Ersfeld, J. Farmer, E. Brunetti, R. Issac, G. Raj, G. Welsh, S. Wiggins, and D. A. Jaroszynski, New J. Phys. **13**, 063042 (2011).
[22]A. A. Andreev, C. Riconda, V. T. Tikhonchuk, and S. Weber, Phys. Plasmas **13**, 053110 (2006).
[23]D. W. Forslund, J. M. Kindel, and E. L. Lindman, Phys. Fluids **18**, 1002 (1975).
[24]P. N. Guzdar, C. S. Liu, and R. H. Lehmberg, Phys. Plasmas **3**, 3414 (1996).
[25]C. Riconda, S. Weber, L. Lancia, J. R. Marques, G. A. Mourou, and J. Fuchs, Phys. Plasmas **20**, 083115 (2013).
[26]G. Lehmann, F. Schluck, and K. H. Spatschek, Phys. Plasmas **19**, 093120 (2012).
[27]G. Lehmann and K. H. Spatschek, Phys. Plasmas **20**, 073112 (2013).
[28]F. Schluck, G. Lehmann, and K. H. Spatschek, Phys. Plasmas **22**, 093104 (2015).
[29]M. Shoucri, J. P. Matte, and F. Vidal, Phys. Plasmas **22**, 053101 (2015).
[30]G. Lehmann and K. H. Spatschek, Phys. Plasmas **23**, 023107 (2016).
[31]L. Lancia, J.-R. Marques, M. Nakatsutsumi, C. Riconda, S. Weber, S. Huller, A. Mancic, P. Antici, V. T. Tikhonchuk, A. Heron, P. Audebert, and J. Fuchs, Phys. Rev. Lett. **104**, 025001 (2010).
[32]S. Weber, C. Riconda, L. Lancia, J. R. Marques, G. A. Mourou, and J. Fuchs, Phys. Rev. Lett. **111**, 055004 (2013).
[33]C. Riconda, S. Weber, L. Lancia, J. R. Marques, G. Mourou, and J. Fuchs, Plasma Phys. Controlled Fusion **57**, 014002 (2015).
[34]L. Lancia, A. Giribono, L. Vassura, M. Chiaramello, C. Riconda, S. Weber, A. Castan, A. Chatelain, A. Frank, T. Gangolf, M. N. Quinn, J. Fuchs, and J. R. Marques, Phys. Rev. Lett. **116**, 075001 (2016).
[35]B. Ersfeld and D. A. Jaroszynski, Phys. Rev. Lett. **95**, 165002 (2005).
[36]R. A. Cairns, J. Plasma Phys. **76**, 395 (2010).
[37]I. Y. Dodin, G. M. Fraiman, V. M. Malkin, and N. J. Fisch, J. Exp. Theor. Phys. **95**, 625 (2002).
[38]Yu. A. Tsidulko, V. M. Malkin, and N. J. Fisch, Phys. Rev. Lett. **88**, 235004 (2002).
[39]N. A. Yampolsky, V. M. Malkin, and N. J. Fisch, Phys. Rev. E **69**, 036401 (2004).
[40]G. Lehmann, K. H. Spatschek, and G. Sewell, Phys. Rev. E **87**, 063107 (2013).
[41]W. P. Yao, B. W. Li, L. H. Cao, F. L. Zheng, T. W. Huang, C. Z. Xiao, and Milos M. Skoric, Laser Part. Beams **32**, 583 (2014).
[42]T. D. Arber, K. Bennett, C. S. Brady, A. Lawrence-Douglas, M. G. Ramsay, N. J. Sircombe, P. Gillies, R. G. Evans, H. Schmitz, A. R. Bell, and C. P. Ridgers, Plasma Phys. Controlled Fusion **57**, 113001 (2015).
[43]Z. Toroker, V. Malkin, and N. J. Fisch, Phys. Plasmas **21**, 113110 (2014).
[44]M. R. Edwards, Z. Toroker, J. M. Mikhailova, and N. J. Fisch, Phys. Plasmas **22**, 074501 (2015).
[45]J. P. Farmer and A. Pukhov, Phys. Rev. E **92**, 063109 (2015).
[46]G. M. Fraiman, N. A. Yampolsky, V. M. Malkin, and N. J. Fisch, Phys. Plasmas **9**, 3617 (2002).
[47]V. Malkin and N. J. Fisch, Phys. Rev. Lett. **99**, 205001 (2007).
[48]V. M. Malkin, Z. Toroker, and N. J. Fisch, Phys. Plasmas **19**, 023109 (2012).
[49]V. M. Malkin, Z. Toroker, and N. J. Fisch, Phys. Plasmas **21**, 093112 (2014).